Journal of Catalysis 301 (2013) 175–186

Contents lists available at SciVerse ScienceDirect

Journal of Catalysis

journal homepage: www.elsevier.com/locate/jcat

Ruthenium-catalyzed hydrogenation of levulinic acid: Influence of the support and solvent on catalyst selectivity and stability

Wenhao Luo [a], Upakul Deka [a], Andrew M. Beale [a], Ernst R.H. van Eck [b], Pieter C.A. Bruijnincx [a,*], Bert M. Weckhuysen [a,*]

[a] Inorganic Chemistry and Catalysis Group, Debye Institute for Nanomaterials Science, Utrecht University, Universiteitsweg 99, 3584 CG Utrecht, The Netherlands
[b] Institute for Molecules and Materials, Radboud University Nijmegen, Heyendaalsweg 135, 6525 AJ Nijmegen, The Netherlands

ARTICLE INFO

Article history:
Received 8 December 2012
Revised 2 February 2013
Accepted 5 February 2013
Available online 20 March 2013

Keywords:
Levulinic acid
Zeolites
Ruthenium
Deactivation
Pentanoic acid
Dealumination

ABSTRACT

The catalytic performance of 1 wt% Ru-based catalysts in the hydrogenation of levulinic acid (LA) has been studied at 40 bar H_2 and 473 K. This was done by assessing the influence of the support acidity (i.e., Nb_2O_5, TiO_2, H-β, and H-ZSM5) and solvent (i.e., dioxane, 2-ethylhexanoic acid (EHA), and neat LA). The Ru/TiO_2 gave excellent selectivity to γ-valerolactone (GVL) (97.5%) at 100% conversion and was remarkably stable even under severe reaction conditions. Ru/H-ZSM5 showed a 45.8% yield of pentanoic acid (PA) and its esters in dioxane, which is the first example of this one-pot conversion directly from LA at 473 K. The gradual deactivation of zeolite-supported catalysts in EHA and neat LA was mainly caused by dealumination, as confirmed by ^{27}Al MAS NMR. Coke buildup originated from angelicalactone and, remarkably, occurred preferentially in the zigzag channels of H-ZSM5 as shown by systematic shifts in the XRD patterns. The GVL ring-opening step is considered to be the rate-determining step on the pathway to PA, necessitating an acidic support.

1. Introduction

Levulinic acid (LA) has been identified as a promising, sustainable platform molecule as it can be produced easily and economically from lignocellulosic biomass via a simple and robust hydrolysis process [1–3]. LA can be further converted into many valuable derivatives of which the conversion to γ-valerolactone (GVL) has been studied most. GVL can find use as a renewable solvent, fuel additive or can be subsequently converted into a whole slate of valuable chemicals, such as 1,4-pentanediol (PD), methyltetrahydrofuran (MTHF), pentanoic acid (PEA), pentanoic acid (PA), or its esters (PE) [4–6]. The various routes to value-added chemicals and fuel components from LA by sequential hydrogenation, (de)hydration, and hydrogenolysis reactions are depicted in Scheme 1. LA can be converted to GVL via either dehydration to angelicalactone (AL) followed by reduction or via reduction to 4-hydroxypentanoic acid (4-HPA) and subsequent dehydration. These reactions are generally performed at a moderate reaction temperature in the range of 298–523 K with hydrogen pressures from 1 to 150 bar. Many examples of commercial heterogeneous ruthenium catalysts on neutral supports, mostly Ru/C, were reported to catalyze the conversion of LA into GVL in different solvents, such as water [7], alcohols [8,9], dioxane [10], and supercritical CO_2 [11]. Less attention has been devoted to the second part of Scheme 1, in which GVL is further converted to the depicted deeper hydrogenation products. GVL can, for instance, be further reduced to 1,4-pentanediol (PD) and subsequently dehydrated to MTHF [4], a process for which high yields were reported over a PtRe/C catalyst [12].

Recently, two new directions have been proposed for the valorization of LA via the alternative PEA pathway. Lange et al. [6] reported on the production of so-called valeric (pentanoic) biofuels, via Pt/TiO_2-catalyzed LA hydrogenation to GVL, followed by GVL hydrogenation to PA over Pt/H-ZSM-5 and finally esterification to give the desired pentanoic acid esters (PE). Related to this are two patents by the Shell laboratories in which a two-step process of LA to GVL followed by GVL to PA conversion is described. A 70% yield of PA was in this case achieved with a $Pt/H\text{-}ZSM\text{-}5/SiO_2$ catalyst [13]. PA and PE could also be obtained in 62% yield in a direct one-pot reaction from ethyl levulinate over a Ru/H-β/silica catalyst [14].

The Dumesic group, on the other hand, has shown that GVL can be converted to PA over a bifunctional metal/acid catalyst, such as Pd/Nb_2O_5, after which PA can be upgraded to 5-nonanone by ketonization [7]. In both approaches, a combination of acid functionality and hydrogenation function is sought to reduce the oxygen content and produce better suited fuel components by ring opening, dehydration, or hydrogenation. Alternatively, Dumesic and

* Corresponding authors. Fax: +31 30 251 10 27 (B.M. Weckhuysen).
E-mail addresses: p.c.a.bruijnincx@uu.nl (P.C.A. Bruijnincx), b.m.weckhuysen@uu.nl (B.M. Weckhuysen).

0021-9517/$ - see front matter © 2013 Elsevier Inc. All rights reserved.
http://dx.doi.org/10.1016/j.jcat.2013.02.003

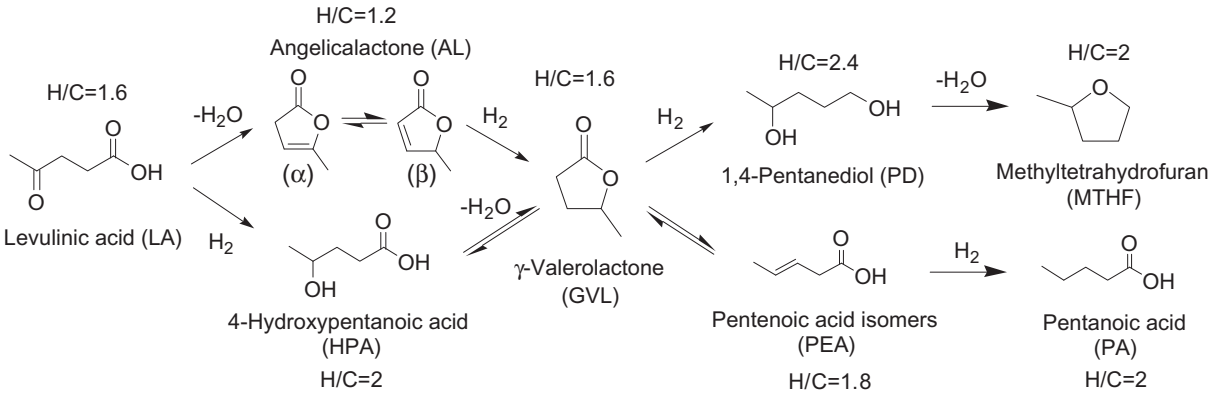

Scheme 1. Hydrogenation platform of levulinic acid (H/C: hydrogen-to-carbon ratio of each compound).

coworkers also reported an integrated strategy for the production of C_{8+} alkenes via GVL ring opening to PEA, followed by decarboxylation and oligomerization of the obtained butenes [15]. This ring-opening/decarboxylation sequence does not require hydrogen and is catalyzed by an acidic catalyst, SiO_2/Al_2O_3, in the absence of a metal hydrogenation function [16].

Indeed, many examples of heterogeneous catalysts are now available for the selective conversion of LA to GVL, most of which use a hydrogenating metal (preferably ruthenium) on a neutral support, usually under dilute and mild solvent conditions. Furthermore, the Shell and Dumesic examples of using a metal on an acidic support for the ring-opening/hydrogenation of GVL to PA show the potential of the PEA pathway for the valorization of levulinic acid. Building on these promising results, the direct, one-pot reaction of LA to PA, without isolation of the GVL intermediate, would be desired to further simplify the process. To achieve this, more insight is required into the influence of the support, in particular the role of support acidity, on selectivity in LA hydrogenation. In addition, the stability of the catalyst, both of the metal component as well as the support, should be assessed under the harsh conditions that can be expected for a highly polar and corrosive LA conversion process. Here, we present the activity, selectivity, and stability of four 1 wt% ruthenium catalysts on non-acidic (Nb_2O_5 and TiO_2) and strongly acidic (H-ZSM5 and H-β) supports in the hydrogenation of LA under increasingly harsh conditions, using dioxane, 2-ethylhexanoic acid, and neat LA as solvents. It was found that zeolite-supported catalysts are capable of the direct synthesis of PA from LA in a one-pot reaction without isolation of the intermediate GVL. An extensive characterization study of the fresh and spent catalysts provided insight into the stability and related deactivation of the catalyst materials under investigation.

2. Experimental section

2.1. Catalyst preparation

Four 1 wt% Ru catalysts on supports of different acidity were prepared. The supports were treated as follows before wet impregnation: TiO_2 (P25, Evonik) was dried at 393 K for 4 h; Nb_2O_5 was obtained by calcination of niobic acid (HY-340, CBMM) at 673 K for 4 h under air flow with a temperature ramp of 10 K/min; H-ZSM5 and H-β (H-ZSM5: CBV2314, Si/Al = 11.5; H-β: CP814E, Si/Al = 12.5, Zeolyst) were converted into the H-form by heating the samples at 1 K/min to 393 K for 1 h and at 2 K/min to 823 K for 4 h. The 1 wt% supported ruthenium catalysts were prepared by wet impregnation using aqueous solutions of ruthenium nitrosyl nitrate ($RuNO(NO_3)_3$, Alfa Aesar). After evaporation of the water, the catalysts were dried at 333 K overnight, calcined at 723 K for 4 h with a heating ramp 2 K/min under N_2 (100 mL/min), followed by reduction at 673 K, for 6 h, under H_2 flow (80 mL/min).

2.2. Catalyst characterization

2.2.1. Temperature-programmed desorption

Catalyst acidity was investigated by temperature-programmed desorption (TPD) of NH_3 under He flow (25 mL/min) using a Micromeritics AutoChem II equipped with a TCD detector. 0.15–0.2 g of catalyst was loaded and dried at 873 K for 1 h, after which the sample was cooled down to 373 K. Subsequently, pulses of ammonia were introduced up to saturation of the sample. The temperature-programmed desorption was performed up to 873 K, with a heating ramp of 5 K/min. The total number of acid sites (mmol NH_3/g zeolite) was determined from the total amount of desorbed ammonia.

2.2.2. Physisorption measurements

N_2 physisorption isotherms were recorded to determine surface areas and pore volumes using a Micromeritics Tristar 3000 setup operating at 77 K. All samples were outgassed for 12 h at 473 K in a nitrogen flow prior to the physisorption measurements. BET surface areas were determined using 10 points between 0.06 and 0.25. Micropore volumes (cm^3/g) were determined by *t*-plot analysis for *t* between 3.5 and 5.0 Å to ensure inclusion of the minimum required pressure points.

2.2.3. Atomic absorption spectrophotometry

The liquid phase was tested after reaction by flame atomic absorption spectrophotometry (AAS) for the presence of Ru and Al. All elements (Ru, Al, Fe, and Cr) were analyzed on a ContrAA 700 apparatus using the following conditions: Ru: 349.9 nm (air/acetylene flame); Al: 396.1 nm (N_2O/acetylene flame); Fe: 248.3 nm (air/acetylene flame); Cr: 357.9 nm (N_2O/acetylene flame).

2.2.4. Thermal gravimetric analysis

Thermal gravimetric analysis (TGA) coupled to mass spectrometry (MS) was performed with a Perkin–Elmer Pyris 1 apparatus. The sample was initially heated to 423 K for 1 h with a temperature ramp of 10 K/min in a 20 mL/min flow of argon to exclude physisorbed water and acetone, followed by a ramp of 5 K/min to 873 K in a 10 mL/min flow of oxygen to burn off the coke. Analysis was performed with a quadrupole Pfeiffer Omnistar mass spectrometer, which was connected to the outlet of the TGA apparatus. Ion currents were recorded for *m*/*z* values of 18 and 44.

2.2.5. Transmission electron microscopy

Transmission electron microscopy (TEM) measurements in bright field mode were conducted with a Tecnai 20FEG microscope operating at 200 kV. The ruthenium particle diameters (more than 200 particles for each sample) were measured using iTEM software (soft Imaging System GmbH). For non-symmetrical particle shapes, both the largest and the shortest diameter was measured to obtain an average value.

2.2.6. X-ray diffraction

Powder X-ray diffraction (XRD) patterns were measured with a Bruker D2 and D8 Advance powder X-ray diffractometer equipped with automatic divergence slits, a Vantec detector and a cobalt $K\alpha_{1,2}$ (λ = 1.78897/1.79026 Å) source. Diffraction patterns were collected between 5–40 or 5–55 2θ (°) with an increment of 0.017 (in 2θ) and an acquisition time of 1 s per step. Unit cell parameters on Ru/H-ZSM5 samples were obtained by performing Le Bail extractions between 5 and 29 2θ (°) using the Rietica LHPM package. Background corrections on all patterns were performed using a 5th order polynomial. The peak profile parameters were calculated using a pseudo-Voigt function. The initial lattice parameters were taken from the IZA database (www.iza-structure/database) for the MFI framework. Silicon (NBS 640) was used as an internal standard, physically mixed with the powdered samples in each measurement. To account for 2θ shifts caused by instrumental errors, that is, sample height or displacement, the Si (1 1 1) reflection was centered at 33.149 2θ for all patterns before performing any analysis.

2.2.7. Infrared spectroscopy

FT-IR spectra were recorded on a Perkin–Elmer 2000 instrument after pyridine desorption at various temperatures. Self-supported catalyst wafers (12–19 mg/16 mm) were pressed at 3 kbar pressure for 10 s. The wafer was placed inside a synchrotron cell with a CaF_2 window. The cell was evacuated to 10^{-6} bar followed by drying of the sample at 573 K (3 K/min) for 1 h. The cell was cooled down to 323 K, and the sample was brought into contact with pyridine vapors (3.1 mbar) for 10 s, kept for 30 min to reach equilibrium, and followed by vacuum for 30 min in order to remove physisorbed and loosely bound pyridine. FT-IR spectra were recorded under vacuum at different temperature (3 K/min) from 323 to 723 K. For each spectrum, 25 scans were recorded with a resolution of 4 cm^{-1}.

2.2.8. Nuclear magnetic resonance

^{27}Al nuclear magnetic resonance (NMR) measurements were performed on a 600 MHz Varian solid-state NMR spectrometer using a 1.6 mm T3 design probe. The probe was tuned to 599.99 MHz for protons and 156.341 MHz for ^{27}Al. Magic angle spinning at 25 kHz was employed. All samples were weighed to enable quantitative measurements. T_1 saturation recovery experiments showed that a repetition time of 0.4 s was more than sufficient for all magnetization to relax back to Boltzmann equilibrium. To ensure that intensities are quantitative regardless of the quadrupole coupling constant [17], the single-pulse measurements were done using rf-field strength of 10 kHz and a pulse length of 2 μs (equaling a tip angle of 7°). Proton decoupling did not improve spectral quality in the 1D experiments. Care was taken to subtract the small background signal from the MAS rotor, prior to integration of the spectra. Intensities were also corrected for the presence of a small amount of satellite sideband intensity that overlaps with the central transition signal by reducing the intensity by an amount equal to the intensity of the ±1 sideband; however, this did not change relative intensities significantly.

Relative amounts of aluminum were obtained by integrating the 1D spectra. The limits of integration were determined with 3QMAS spectra (see Fig. S11 for an example) and set to a range from −20 to 8 ppm for octahedral aluminum (Al(VI)), 8–41 ppm for penta-coordinated aluminum (Al(V)), and 41–70 ppm for tetrahedral aluminum (Al(IV)) for Ru/H-β. For both Ru/H-ZSM5 samples, only a trace amount of Al(V) was detected in the 3QMAS, while the Al(IV) signal extended down to 20 ppm. Hence, integration limits were set from −20 to 20 ppm for Al(VI) and 20 to 70 ppm for Al(IV) for these samples.

2.3. Catalyst testing

In a typical reaction, the batch autoclave reactor was loaded with catalyst, substrate, and solvent, purged three times with argon after which the reaction mixture was heated to reaction temperature and charged with H_2 to 40 bar. This was taken as the starting point of the reaction. After the reaction was cooled to room temperature, the H_2 was released, and 2 wt% anisole was added as internal standard. The catalyst was separated by centrifugation, filtration, and finally washed with acetone. The reaction products were analyzed using a Shimadzu GC-2010A gas chromatograph equipped with a CP-WAX 57-CB column (25 m × 0.2 mm × 0.2 μm) and FID detector. Products were identified with a GC−MS from Shimadzu with a CP-WAX 57CB column (30 m × 0.2 mm × 0.2 μm). The gas-phase reaction products were analyzed by an online dual channel Varian CP4900 micro-GC equipped with a COX column and TCD detector, for analysis of H_2, CO_2, CO, and CH_4.

Dioxane runs were performed with 10 wt% levulinic acid (2.5 g, 21.5 mmol) in dioxane (22.5 g) over a series of 1 wt% Ru catalysts (0.3 g) containing different supports. The reactions were run in a 50 mL Parr batch autoclave at a temperature of 473 K for 4 h using a hydrogen pressure 40 bar and a stirring speed of 1600 rpm.

2-Ethylhexanoic acid runs were performed with 10 wt% levulinic acid (6.0 g, 51.7 mmol) in 2-ethylhexanoic acid (54 g) with 1 wt% Ru catalysts (0.6 g). The reactions were run in 100 mL Parr batch autoclave at a temperature of 473 K for 10 h using a hydrogen pressure 40 bar and a stirring speed of 1600 rpm. 1 mL of solution was sampled at various intervals during the reaction. Reactions with intermediates GVL (2.2 g, 21.5 mmol) or PEA (2.2 g, 21.5 mmol) in EHA (22.8 g) were conducted with 0.3 g of catalyst in the 50 mL Parr batch autoclave.

Finally, neat LA runs were performed with LA (20 g, 172 mmol) over 1 wt% Ru catalysts (0.3 g or 0.5 g). The reactions were run in a 50 mL Parr batch autoclave at a temperature of 473 K for 4 h and 10 h using a hydrogen pressure 40 bar and a stirring speed of 1600 rpm.

3. Results and discussion

3.1. Catalyst characterization

The 1 wt% ruthenium catalysts were synthesized by wet impregnation of the TiO_2, Nb_2O_5, H-ZSM5 (Si/Al 11.5), and H-β (Si/Al 12.5) supports. The fresh catalysts were characterized by XRD, TEM, N_2 physisorption and NH_3-TPD, IR after pyridine adsorption and solid-state ^{27}Al (1D MAS, 2D 3QMAS) NMR. The bright field TEM images of the fresh catalysts (see Fig. S3) show that the average particle sizes of the Ru/TiO_2, Ru/H-ZSM5, and Ru/H-β were very similar and around 3.5 nm mean particle size. Unfortunately, the ruthenium particle size of the Ru/Nb_2O_5 catalyst could not be determined by TEM due to lack of contrast. No Ru phase could be observed in the XRD diffractograms of the fresh catalysts (Fig. S6).

The acid properties, namely the quantity and strength of the acid sites, of the fresh catalysts were determined by NH_3-TPD. Table 1 lists the total amount of acidic sites of the four catalysts

under investigation, as well as a distinction between weak and strong acid sites. Woolery et al. attributed the TPD peak at high temperature to Brønsted acid sites (strong acid) connected with framework Al (FAl) sites and the low temperature peak to extra-framework Al species (EFAl), which act as Lewis acid sites (weak acid) [18]. Here, the low- and high-temperature regions are defined as 373–523 K and 523–673 K, respectively (Fig. S2). The differences in acidity between the different catalysts are evident both from the amount and from the strength of the acid sites, with acidity decreasing in the order: Ru/H-ZSM5 > Ru/H-β > Ru/TiO_2 > Ru/Nb_2O_5. Ru/TiO_2 and Ru/Nb_2O_5 can therefore be considered as non-acidic catalysts with only a very small amount of Lewis acid sites and their activity and selectivity in the LA hydrogenation be compared with the strongly acidic zeolite-supported Ru/H-ZSM5 and Ru/H-β catalysts, which have both Brønsted and Lewis acid sites in the respective MFI and BEA framework types.

The surface areas and pore volumes of the catalysts were determined by N_2 physisorption and are listed in Table 2. Of the non-acidic catalysts, Ru/Nb_2O_5 has a larger surface area than Ru/TiO_2, while Ru/H-β has a higher micropore surface and external surface area than Ru/H-ZSM5.

3.2. Catalytic reactions in dioxane

3.2.1. Catalyst performance

The influence of the support on catalytic activity and selectivity was initially screened at 473 K and 40 bar H_2 in dioxane as the solvent. To exclude any influence of external mass transfer limitations, reactions were run at different stirrer speeds (Fig. S1) and to ensure that the hydrogenation reactions take place in the kinetic regime, all experiments were subsequently run at a stirrer speed of 1600 rpm.

Fig. 1 shows the large differences in selectivity between the four supported catalysts in the hydrogenation of a 10 wt% solution of levulinic acid in dioxane. Full conversion of LA was achieved with all catalysts except for Ru/Nb_2O_5. The non-acidic-supported catalysts mainly show formation of GVL (yields of 61.8% for Ru/Nb_2O_5 and 92.3% for Ru/TiO_2) with minor amounts of MTHF (2.6% for Ru/Nb_2O_5 and 2.3% for Ru/TiO_2) and PD (1.7% for Ru/TiO_2), with mass balances of 92.0 and 96.3% for Ru/Nb_2O_5 and Ru/TiO_2, respectively. Trace amounts (<0.1%) of AL (α and β), but no 4-HPA, were detected at the beginning of the reaction (i.e., at low LA conversion levels) with all four catalysts. Ru/TiO_2 showed the highest GVL yield of 92.3% (selectivity = 95.8%) under these conditions. These results are comparable to previously reported GVL yields over Ru/TiO_2 catalysts in various solvents. Corma et al., for instance, obtained a 93.0% yield of GVL after 5 h reaction over a 0.6 wt% Ru/TiO_2 at 423 K, 35 bar hydrogen pressure in water [19]. Palkovits et al. reported a yield of 71.2% after 160 min of reaction time over 5 wt% Ru/TiO_2 at 403 K, 12 bar hydrogen pressure in ethanol and water [9]. Ruthenium supported on the strongly acidic zeolites showed a quite different product distribution. Full conversion is achieved in both cases, but in addition to GVL, the deep hydrogenation product PA and its ester derivatives (PE) were obtained in considerable amounts with Ru on H-ZSM5 or H-β. PD was not observed with the zeolite catalysts, however. The more acidic Ru/H-ZSM5 yielded more PA and PE, but at the expense of a slight increase in loss of mass balance (4% for Ru/H-ZSM5 vs. 3.3% for Ru/H-β). The PE derivatives are the result of esterification of PA with dioxane decomposition products, as the solvent was found not to be fully stable in the presence of the acidic catalysts under the applied conditions. Indeed, decomposition of dioxane (2–4% in total) to ethanol, butanol isomers, and other dioxane-derived small molecules (2-ethoxy-ethanol, diethyl ether) was detected after the runs. The *n*-butanol included in the *n*-butyl ester of pentanoic acid is probably the product of a Guerbet-type reaction of the ethanol formed. The total combined yields of PA and PE from LA are 37.5% with Ru/H-β and 45.8% with Ru/H-ZSM5. These results show that the direct conversion to PA is feasible in a one-pot reaction already at the fairly low temperature of 473 K. Interestingly, a metal/zeolite-catalyzed process from GVL to PA was patented by Shell [14,20], but not a process from LA directly to PA; furthermore, a 62% yield of PA and PE was claimed over a 1 wt% Ru/H-β/silica catalyst at 523 K and 80 bar H_2 with ethyl levulinate rather than LA as the substrate in a batch autoclave reactor [14]. The gas-phase composition of the dioxane runs was also checked by online GC analysis, with only minute amounts of CO and CO_2 (carbon balance <0.03%) being detected, which suggests that decarboxylation, for example, by PA conversion to butene does not occur under the applied reaction conditions.

3.2.2. Catalyst stability

Spent catalysts were extensively characterized to assess stability and detect any changes in either the metal phase or the support. The ruthenium particle sizes and support morphologies of different catalysts were examined by TEM (Fig. S3). The average diameters of the ruthenium particles with standard deviations of the fresh and spent catalysts are given in Fig. 2. The lack of contrast did not allow the particle size to be determined for the niobia samples.

The average Ru particle diameter of the fresh catalysts was around 3.5 nm for all three catalysts. All catalysts showed a small increase in particle size in the spent catalysts to around 4 nm, now with a slightly broader distribution around the mean. In general, the observed sintering after a 4-h reaction in dioxane was limited, though. The increased standard deviation of the spent catalysts nonetheless illustrates that more large Ru particles are formed during reaction with Ru/TiO_2, H-β, and H-ZSM5. The extent of Ru loss to the liquid phase by leaching was determined by AAS after 4 h reaction and found to be marginal. Ru/H-ZSM5 showed the highest loss, but at only 2.4% of the original weight of ruthenium (Table 3).

A comparison of the powder XRD patterns of the fresh and spent catalysts (Fig. S6) showed patterns similar in peak intensity and peak center, indicating that there was no phase change of the supports under the applied conditions and that the zeolites maintained their structural integrity. N_2 physisorption data provided insight into the extent of coke buildup. The formation of carbon residues or coke on the catalyst surface resulted in a decrease in surface area and pore volume (Table 2) for the niobia and zeolite-supported catalysts, but not for the titania-supported one. The results obtained in dioxane thus show large selectivity differences for the ruthenium catalysts on supports of different acidity,

Table 1
Acid concentrations calculated from NH_3-TPD.

Catalyst	Total acidity (mmol/g_{cat})	Low *T* region (mmol/g_{cat})	High *T* region (mmol/g_{cat})
Ru/H-ZSM5	1.35	0.93	0.42
Ru/H-β	1.07	0.71	0.36
Ru/TiO_2	0.26	0.26	0
Ru/Nb_2O_5	0.14	0.14	0

Table 2
N_2 physisorption data of the fresh and spent catalyst materials under investigation.

	Catalyst	BET(m^2/g)	Micropore surface area (m^2/g)	External surface area (m^2/g)	Micropore volume (cm^3/g)[a]	Coke contents (wt%)[b]
Fresh	Ru/Nb_2O_5	98		98		
	Ru/TiO_2	56		56		
	Ru/H-β	515	329	184	0.161	
	Ru/H-ZSM5	343	258	85	0.126	
Spent, 4 h in dioxane	Ru/Nb_2O_5	70		70		
	Ru/TiO_2	55		55		
	Ru/H-β	436	264	172	0.129	
	Ru/H-ZSM5	229	182	47	0.090	
Spent, 10 h in EHA	Ru/Nb_2O_5	55		55		1.3
	Ru/TiO_2	54		54		0.8
	Ru/H-β	478	292	180	0.143	3.4
	Ru/H-ZSM5	152	116	36	0.057	5.5
Spent, 10 h in LA	Ru/TiO_2	52		52		1.8
	Ru/H-β	373	200	172	0.098	10.7

[a] Data obtained by the *t*-plot method.
[b] Data determined by TGA.

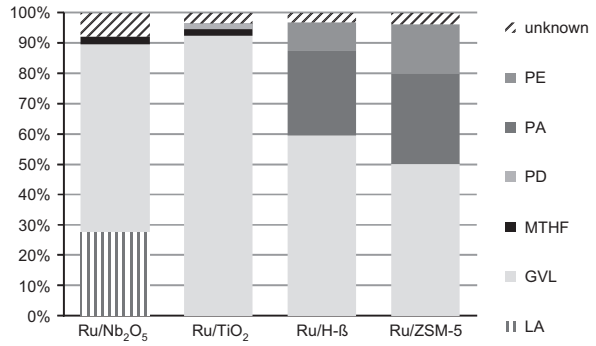

Fig. 1. Catalytic hydrogenation of 10 wt% levulinic acid in dioxane at 473 K, 40 bar, 4 h of reaction time, 1 wt% Ru on different supports, stirrer speed 1600 rpm. LA: levulinic acid; GVL: γ-valerolactone; MTHF: methyltetrahydrofuran; PD: 1,4-pentanediol; PA: pentanoic acid; PE: pentanoic acid esters (butyl pentanoate isomers, 2-ethoxyethyl pentanoate and valeric pentanoate); and unknown: missing mass balance.

while the limited leaching and sintering points at good catalyst stability under the applied reaction conditions.

3.3. Catalytic reactions in 2-ethylhexanoic acid

The reactions run in dioxane were well suited for initial studies into the selectivity, activity, and stability of the catalysts, but the use of this particular solvent also showed to have some disadvantages. In particular, in the presence of the strongly acidic catalysts, dioxane was found to be unstable, hampering product analysis due to dioxane-derived byproduct formation, that is, the pentanoic acid esters. The use of an alternative solvent could alleviate this and would also provide an opportunity to subject the catalysts to harsher conditions to further assess their stability under the typically highly polar and acidic conditions encountered in a more commercial levulinic acid conversion process. With this in mind, 2-ethylhexanoic acid (EHA) was selected as solvent. EHA is stable under the typical hydrogenation conditions and, having a similar pK_a, is a good mimic of LA. This allowed the study of catalyst activity and selectivity in the conversion of LA, but, importantly, also of intermediates such as GVL. In addition, catalyst stability under conditions that are similar to running the reaction in neat LA could be determined. The latter is important as supported metal catalysts can suffer from leaching of both the metal phase as well as of the support under the corrosive and highly polar liquid-phase conditions typically employed in the conversion of renewable platform

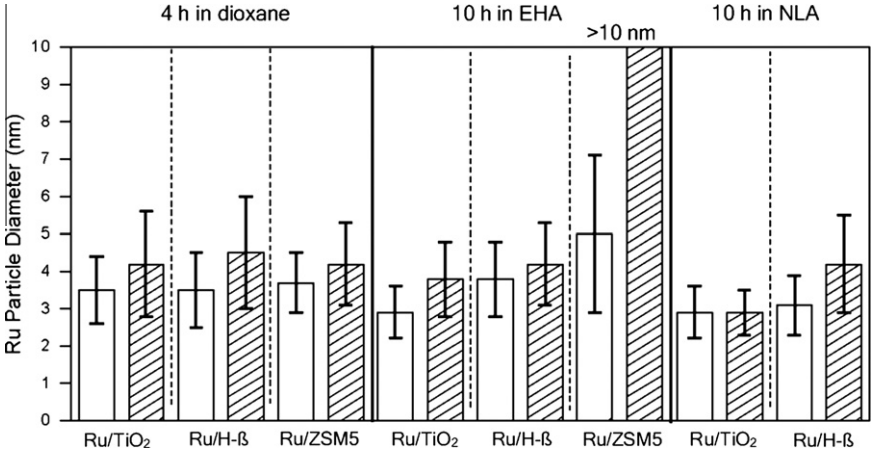

Fig. 2. Ru particle size (nm) determined by TEM for the fresh and spent catalysts after reaction in dioxane, 2-ethylhexanoic acid (EHA) and neat levulinic acid (NLA) (blank pattern: fresh catalyst; and diagonal pattern: spent catalyst).

Table 3
Ruthenium leaching after reaction in dioxane, 2-ethylhexanoic acid (EHA) and neat levulinic acid (LA) as determined by AAS of the liquid phase after reaction.

Spent catalyst	Ru leaching, 4 h in dioxane (%)	Ru leaching, 10 h in EHA (%)	Ru leaching, 10 h in neat LA (%)
Ru/TiO_2	2.1	2.9	0.5
Ru/Nb_2O_5	1.8	0.9	–
Ru/H-β	1.6	0.7	0.5
Ru/H-ZSM5	2.4	0.9	–

molecules such as LA, and more insight is needed into possible deactivation pathways.

3.3.1. Catalyst performance

Concentration profiles of substrate and products are depicted in Fig. 3. As with the runs in dioxane, clear differences in selectivity and activity are observed. Both the Ru/Nb_2O_5 and the Ru/TiO_2 catalysts are highly selective for GVL in EHA, with only very small amounts of MTHF formed as the only byproduct (<1 mol%). The reaction over Ru/TiO_2 is faster, however, as full conversion is obtained after 4 h, while 2.4 mol% of LA was still left after 5 h reaction with the Ru/Nb_2O_5 catalyst. The Ru/H-β catalyst also showed full LA conversion in 4 h, while Ru/H-ZSM5 is the fastest catalyst achieving full LA conversion in only 3 h. The activity of the catalyst is illustrated by the turnover frequencies (TOF) (at LA conversions of ~20%), which follow the sequence: Ru/H-ZSM5 (0.204 s^{-1}) > Ru/TiO_2 (0.164 s^{-1}) > Ru/H-β (0.131 s^{-1}) > Ru/Nb_2O_5 (0.088 s^{-1}).

Only GVL is observed as the product for both the Ru/Nb_2O_5 and the Ru/TiO_2 catalysts as the support is too weakly acidic to open the ring of GVL under the applied conditions. The acid-supported catalysts Ru/H-ZSM5 and Ru/H-β again showed the formation of the deep hydrogenation product PA with PA yields of 15.5% (Ru/H-ZSM5) and 6.3% (Ru/H-β) after 10 h of reaction. Again, only minute amounts of MTHF (<1%) were detected, and no PD was observed. The PA yields in EHA were lower than those observed in dioxane, illustrating that the substrate LA and the intermediate GVL, which is the precursor to PA, compete with the solvent for adsorption on or interaction with the catalyst. Related to this, the extent and origin of catalyst deactivation is different in this solvent (see below). The data thus illustrate that while the influence of the

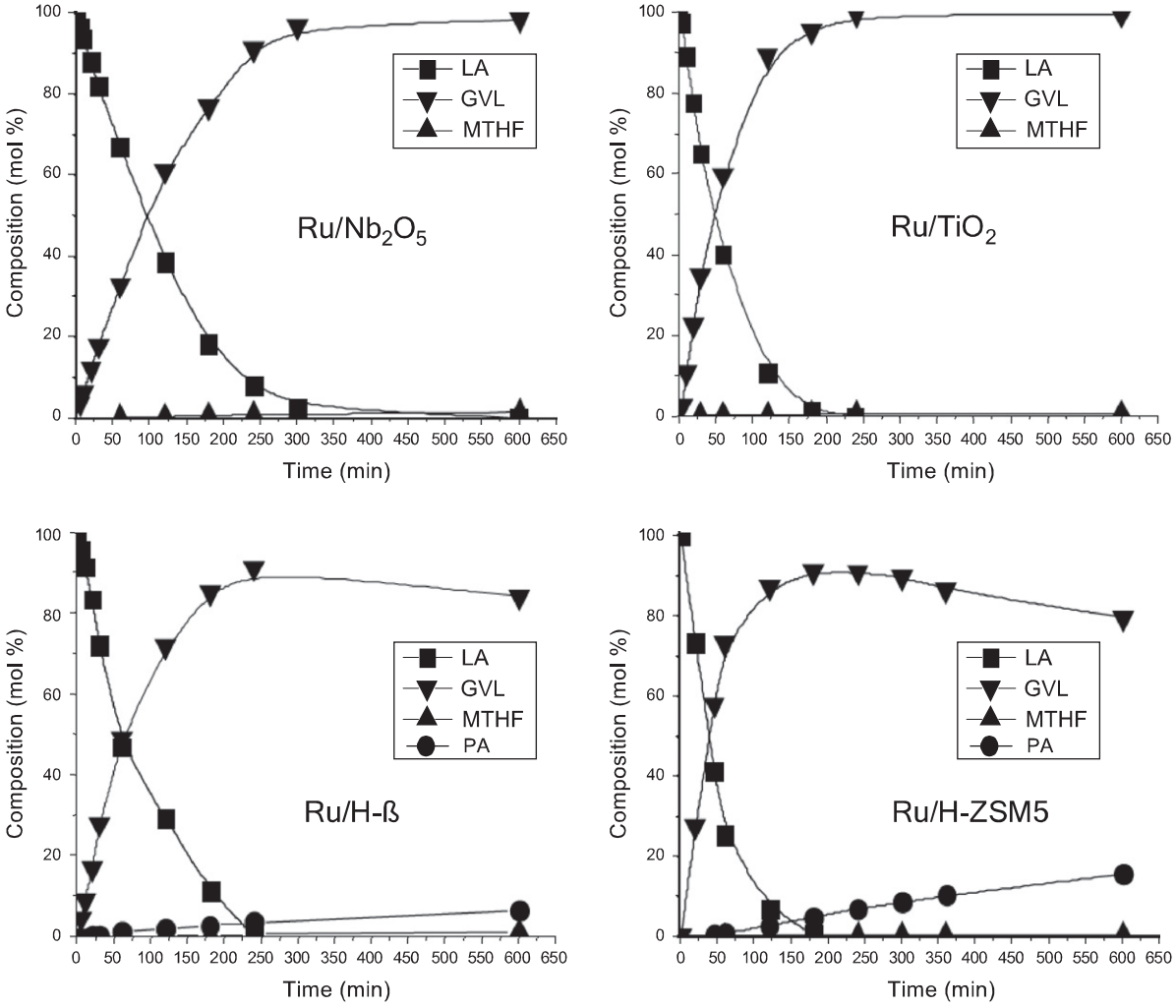

Fig. 3. Time profiles of the catalytic hydrogenation of 10 wt% levulinic acid in 2-ethylhexanoic acid. Conditions: 473 K, 40 bar, 10 h of reaction time, 1 wt% Ru loading with different supports, stirrer speed of 1600 rpm LA: levulinic acid; GVL: γ-valerolactone; MTHF: methyltetrahydrofuran; PA: pentanoic acid.

acid functionality is rather subtle in the first LA to GVL step, the strong acid sites on the zeolites are clearly required for the consecutive GVL to PA conversion.

The selectivity patterns of the different catalysts are compared at different LA conversion levels in Fig. 4. At low LA conversion (~30%), all catalysts show high GVL selectivity (S_{GVL} > 97%), with only Ru/H-β producing already some PA. No PA is observed at this point with Ru/H-ZSM5, which might be attributed to a more limited accessibility of GVL to the acid sites in H-ZSM5. Increasing LA conversion (~60% and 90%) leads to increased selectivity for PA over the acidic zeolite supports, with GVL selectivity still over 98% for the less acidic supports TiO_2 and Nb_2O_5. Full LA conversion was achieved after 10 h of reaction with all catalysts. Although Ru/H-β initially produced more PA, PA selectivity was lower for Ru/H-β than for Ru/H-ZSM5 after 10 h, suggesting that deactivation is more rapid for Ru/H-β than for Ru/H-ZSM5 (see below).

3.3.2. Hydrogenation of intermediates

As is clear from the LA hydrogenation results presented above, the gradual catalyst deactivation limits the yield of PA under these more severe conditions. To get more insight into the inherent ability of the zeolite-supported catalysts to catalyze the steps after GVL formation, that is, ring opening and hydrogenation to PA, reactions with the implicated intermediates GVL and PEA were also performed in EHA. Ru/TiO_2 and Ru/H-β were chosen to compare the non-acid and acid-supported catalysts (Table 4).

As expected, PA was not observed with Ru/TiO_2 after 4 h or even 10 h of reaction (Table 4, entries 1–3). Ru/H-β slowly, but cleanly converts GVL to PA in EHA, with a yield of 7.2% after 15 min, which increases to 34.0% after 10 h. This PA yield is higher than the one obtained in the LA run, pointing at the key role of the acid sites in the GVL to PA conversion and partial deactivation by acid-site loss (be it due to blockage or dealumination) in the first LA to GVL step (Table 4, entries 4–9).

Unexpectedly, a standard check of the activity of the support itself in the reaction (Table 4, entries 10, 11, 13), showed that PA was also obtained with only H-β present. Trace amounts of residual Ru were held responsible for this hydrogenation activity, but the (limited) activity of just H-β remained even after extensive dismantling and cleaning of the batch autoclave. AAS analysis of the liquid phase after reaction did not detect any Ru or Cr [21], but trace amounts of iron were found (Table S1). The activity in the blank reactions with just the zeolite support is thus attributed to acid-catalyzed ring opening by the zeolite to form PEA, which is subsequently hydrogenated to PA by any iron leached from the autoclave walls. Indeed, runs with PEA showed hydrogenation activity to yield some PA in the absence of the zeolite (Table 4, entry 16), while in the presence of the zeolite, equilibration with GVL as well as PA formation were observed. Importantly, blank reactions (no support, no catalyst) did not show any conversion (Table 4, entries 14 and 15). The background hydrogenation reaction therefore does not influence the catalytic results as it is much slower than the Ru/zeolite-catalyzed hydrogenation reactions. These results show that ring opening is the rate-limiting step in the GVL to PA conversion and that PEA hydrogenation is very straightforward. Furthermore, ring opening from GVL to PEA is reversible (entry 17) with the equilibrium

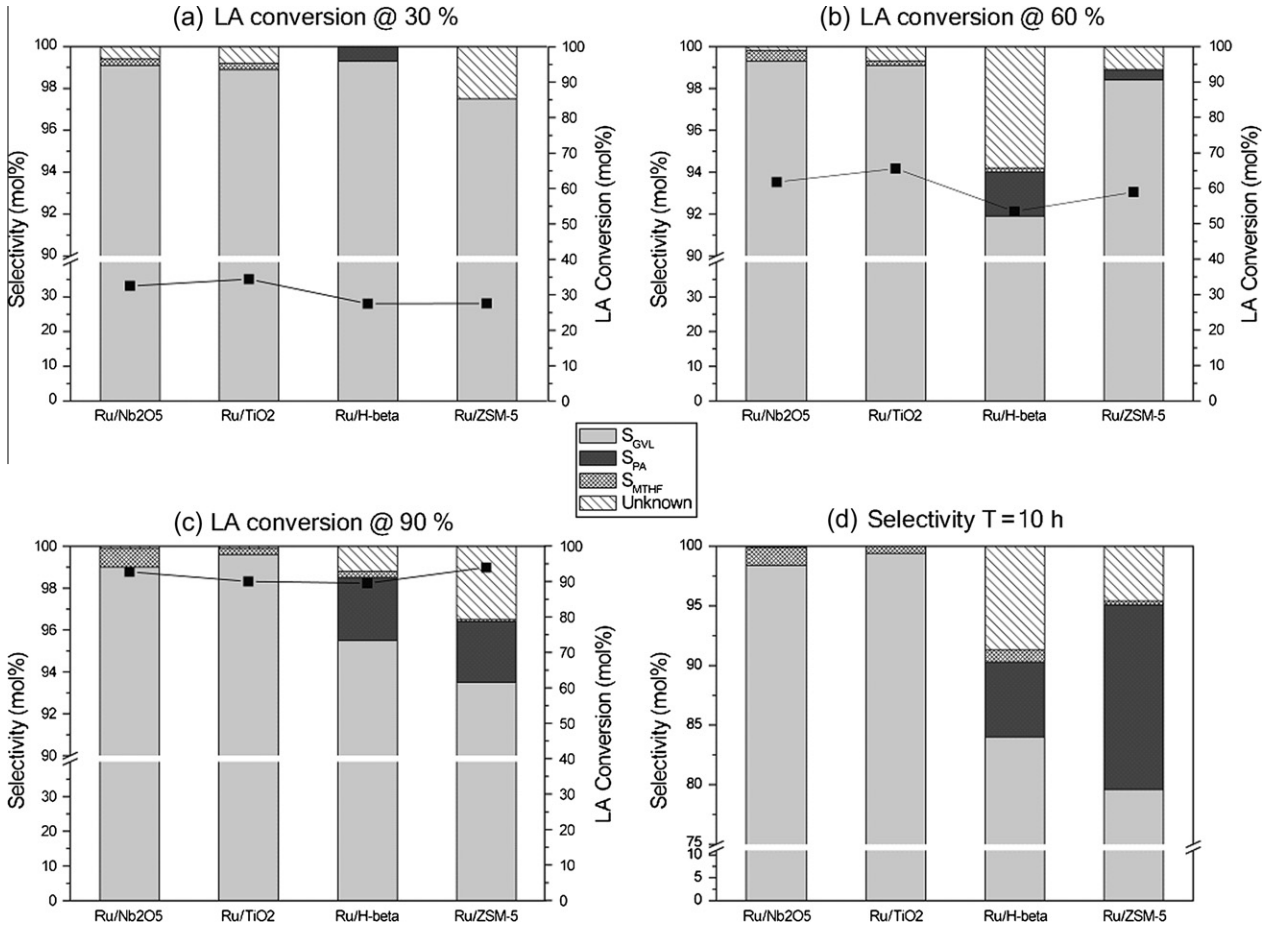

Fig. 4. Selectivity comparison of different catalysts at different levulinic acid (LA) conversion levels; LA conversion at: (a) 30%; (b) 60%; (c) 90%; (d) after 10 h of reaction time with full conversion of LA.

Table 4
Results for the catalytic hydrogenation of γ-valerolactone (GVL) or pentanoic acid (PEA) in 2-ethylhexanoic acid (PA, pentanoic acid; and MTHF, methyltetrahydrofuran).

Entry	Catalyst	Time (h)	C-balance (%)	GVL conv. (%)	PA yield (%)	MTHF yield (%)	PEA yield (%)
GVL							
1	Ru/TiO_2	4	97.9	2.3	0	0.2	0
2	Ru/TiO_2	10	95.8	4.9	0	0.7	0
3	TiO_2	4	99.9	0.2	0	0.1	0
4	Ru/H-β	0.25	94.5	12.7	7.2	0	0
5	Ru/H-β	1	92.5	17.3	9.8	0	0
6	Ru/H-β	2	93.8	23.1	16.9	0	0
7	Ru/H-β	3	93.7	26.7	20.4	0	0
8	Ru/H-β	4	95.1	28.7	23.7	0.1	0
9	Ru/H-β	10	93.7	40.5	34.0	0.2	0
10	H-β	4	96.3	17.6	11.0	0	2.9
11	H-β	4	97.1	19.2	14.8	0	1.3
12	H-ZSM5	4	99.3	6.0	5.3	0	0
13	H-β	10	95.2	30.0	23.2	0	2.0
14	No Cat	4	102.9	-2.8	0	0.1	0
15	No Cat	10	99.6	0.6	0	0.2	0
		Time (h)	C-balance (%)	PEA conv. (%)	PA Yield (%)	GVL yield (%)	
PEA							
16	H-β	4	99.3	99.6	18.0	80.9	
17	No Cat	4	99.9	15.5	12.1	3.3	

Conditions: 473 K, 40 bar, 1 wt% Ru on different supports, stirrer speed of 1600 rpm, 21.6 mmol of GVL or PEA in EHA (equimolar to 10 wt% LA).

favoring GVL under the applied conditions. H-β showed higher yield of PA than H-ZSM5 (Table 4, entries 10–12), further pointing at the better accessibility of the acid sites in the larger pore H-β.

The gradual deactivation of the catalyst, in particular with respect to its ability to catalyze the second GVL to PA conversion, is illustrated by a longer 24 h run with Ru/H-β in which additional fresh catalyst was added after 4 and 14 h of reaction. Changes in composition of the liquid phase are depicted in Fig. 5. The reaction was run with half the amount of catalyst (0.3 g) compared to the results in Fig. 5 for Ru/H-β with the second half of catalyst (0.3 g) only being added after 4 h. As a result, conversion dropped from full (0.6 g catalyst) to 68.9% (0.3 g). The yield of PA after 10 h of reaction was higher, however, for the sequential addition experiment (10.1% vs. 6.3%), which shows that the deactivation of the catalyst (by loss of acid sites, see below) happens already in the first stage of the reaction, which is concerned mostly with the conversion of LA to GVL. PA production seems to level off after 10 h, indicating that the acid sites are no longer accessible. Addition of a fresh batch of catalysts restored activity with PA yields increasing almost linearly over the next 14 h.

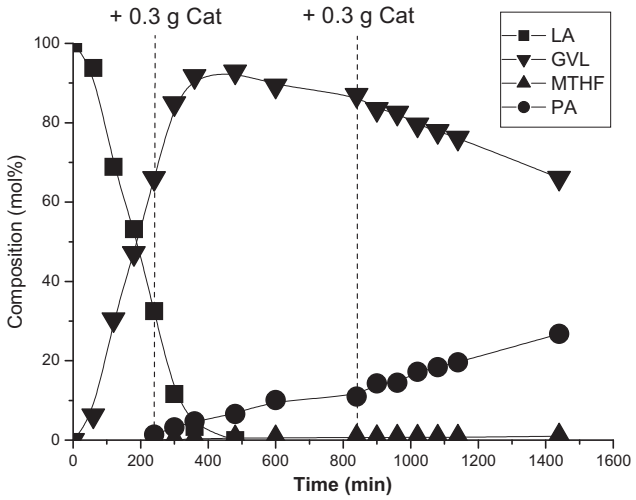

Fig. 5. Catalytic hydrogenation of levulinic acid (LA) and formation of γ-valerolactone (GVL), pentanoic acid (PA) and methyltetrahydrofuran (MTHF) as a function of time at 473 K, 40 bar with 1 wt% Ru/H-β in 2-ethylhexanoic acid with twice the addition of fresh catalyst.

3.3.3. Catalyst stability

The stability of the catalysts under these more severe conditions was again studied by TEM and AAS to quantify any sintering or leaching of ruthenium (Fig. S4, Fig. 2 and Table 3). Similar to the results obtained in dioxane, limited sintering of the Ru particles was observed for the spent Ru/TiO_2 (particle size increase from 2.9 to 3.8 nm, Table 3) and Ru/H-β (3.8–4.5 nm) after 10 h reaction in EHA. Some bigger clusters were found on the spent catalysts, however, causing broadening of the distribution. A major difference with the reactions run in dioxane is that severe sintering was observed for the spent Ru/H-ZSM5 catalyst, as TEM showed that some of the H-ZSM5 particles contained no Ru, while others showed big clusters of Ru, as confirmed by EDX (Fig. S4). Loss of ruthenium to the liquid phase was marginal (<3%), nonetheless, for all four catalysts (Table 3).

3.3.3.1. Coke formation. The lower PA yield that is observed in EHA with the Ru/zeolite catalysts points at deactivation of the catalyst material. In addition to any changes to the metal phase, changes to the support, for example, deactivation by coking, loss of active sites by dealumination, or phase changes can also be expected. TGA measurements did show different extents of coke formation on the different supports (Table 2). More carbon residue or coke is deposited on the acid-supported catalysts. The weight loss measured by TGA decreases in the order of H-ZSM5 > H-β > Nb_2O_5 > TiO_2. N_2 physisorption measurements of the spent catalysts also show a decrease in surface area and pore volume (Table 2). TGA–MS analysis of the spent Ru/H-β catalyst (from a run in neat LA, vide infra) provided some further insight into the probable coke-precursors. Indeed, the H/C ratio, determined from the CO_2 and H_2O MS signals, reaches a plateau at H/C 1.4 (Fig. S10). Given the H/C ratios of the various intermediates in the LA hydrogenation platform (see Scheme 1), AL is the only intermediate with a H/C ratio lower than 1.4 and must therefore be involved in the coke formation (although it is most probably not the sole source). This is further corroborated by the GC and GC–MS results obtained at low conversion, in which AL, but not 4-HPA, is detected in minor amounts.

The XRD patterns of the spent catalysts showed no evidence for formation of new phases after 10 h of reaction in EHA (Fig. S7). Closer inspection of the X-ray diffraction pattern of the spent Ru/H-ZSM5, however, showed a shift of peaks to lower 2θ values (higher corresponding *d*-values), suggesting an expansion of the unit cell (Fig. 6). Considering the respective bond distances of Al–O and

Si–O (~1.75 Å and ~1.61 Å, respectively), dealumination of framework aluminum would result in the opposite effect, that is, a shift of peaks to higher 2θ values (lower d-values) as a result of a "shrinking" unit cell. As also shown by solid-state ^{27}Al NMR, there was indeed loss of aluminum (Fig. 8) in the Ru/H-ZSM5 sample. Further considering the initial amount of Al in the fresh sample (3.1 wt%), this would not be reflected in lattice parameter changes, as was already previously noted [22,23].

However, the porosity studies indicated a significant loss in the internal pore volume of the H-ZSM5 zeolite, which could be associated with possible coke buildup within the zeolite channels. This could lead to an expansion of the unit cell, consistent with the observation from the diffraction patterns. To test this hypothesis further, the spent Ru/H-ZSM5 sample was exposed to a stream of pure oxygen at 723 K for 4 h to remove as much coke from the material as possible. The XRD pattern of the recalcined Ru/H-ZSM5 sample is compared to the fresh and spent material in Fig. 6. Clearly, the pattern corresponding to the spent catalyst is shifted to the right as compared to the fresh catalyst suggesting an "expanded" unit cell for the former. After recalcination of the spent catalysts, the pattern is comparable, however, to the fresh pattern suggesting the unit cells are similar in size. Table 5 lists the lattice parameters obtained for each pattern. While lattice parameter "*a*" remains constant for all three patterns, unit cell parameters "*b*" and "*c*" are seen to change (as expected) over the three samples. The spent sample shows the largest unit cell, while treating the sample in an oxygen-rich feed appears to result in a unit cell comparable to the fresh sample.

It is important to recall that H-ZSM5 is made up of a 3-dimensional porous network with large straight channels that are oriented perpendicular to smaller zigzag channels. From a unit cell perspective, the former are oriented perpendicular to axes *a* and *c*, while the latter are (almost) perpendicular to axes *b* and *c*. Since the analysis shows lattice parameter *a* to be constant and parameters *b* and *c* to increase in the spent sample, it can be deduced that coke forms within the zigzag channels of the zeolite (oriented parallel to axis *a*), which attributes to the deactivation of the catalyst. After treatment in an oxygen-rich flow, most of the coke gets burnt off, and values for *b* and *c* closer to the values seen for the fresh catalyst are again obtained. The preferential deposition of coke in the zigzag channels is further substantiated by the larger shifts of the peaks corresponding to $0kl$ planes compared to peaks corresponding to $h00$ planes.

3.3.3.2. Support dealumination. Although the Ru/H-ZSM5 catalyst showed more coke deposition (Table 2), a lower PA selectivity at low LA conversion level (Fig. 4) and more sintering of Ru (Fig. S4) during the reaction in EHA, a higher yield of PA than with Ru/H-β was still obtained with this catalyst after 10 h of reaction. As the GVL to PA conversion is critically dependent on the acid sites of the zeolite, factors other than active site blockage, for example, loss of active sites by dealumination should therefore also be taken into account. Al loss was studied by IR after pyridine adsorption and solid-state ^{27}Al NMR.

The absorbance FT-IR spectra in Fig. 7 show pyridine adsorbed on the two types of zeolite catalysts. With fresh Ru/H-ZSM5, pyridine adsorption resulted in the formation of protonated (1636, 1489, and 1542 cm^{-1}) and coordinated (1620, 1489, and 1454 cm^{-1}) species [24–26]. The former interaction (specifically the 1542 cm^{-1} vibration) can be assigned to pyridine interacting with a Brønsted acid site (BAS), while the 1454 cm^{-1} vibration is indicative of an interaction with Lewis acid sites (LAS). The decrease in BAS after the 10 h reaction is very limited, as only a slight decrease in intensity of the band at 1542 cm^{-1} is observed, while a small increase in the intensity and a shift to 1450 cm^{-1} of the vibration originally at 1454 cm^{-1} (Fig. 7a) suggests an increase in LAS, probably by framework dealumination [27].

On fresh Ru/H-β, vibrations assigned to adsorbed protonated pyridine (1637, 1490, and 1545 cm^{-1}) and coordinated pyridine (1622, 1490, and 1455 cm^{-1}) is observed as well. After reaction, a decrease in all the bands is seen with spent Ru/H-β, indicating loss of acid sites. The two new bands at 1603 and 1446 cm^{-1} (Fig. 7b) most likely correspond to pyridine adsorbed on a new type of LAS in the spent catalyst, as a result again of dealumination [28]. The severe loss of BAS and LAS can also be seen in the FT-IR spectra of the Ru/H-β catalyst without pyridine, as the bands at 3779 (LAS), 3662 (LAS), and 3607 cm^{-1} (BAS) corresponding to the various OH groups that are observed in the fresh catalyst, disappear after reaction in EHA (Fig. S9).

The 1D ^{27}Al MAS NMR spectra of the fresh and spent Ru/zeolite catalysts are depicted in Fig. 8. The ^{27}Al 3QMAS NMR spectra of fresh and spent Ru/H-ZSM5 show two resonances in both the tetrahedral and the octahedral aluminum region, a broad and a narrow one (see Fig. S11). The sharp resonance at 54 ppm is assigned to tetrahedral framework aluminum species (Al(IV), FAl, BAS), while the broad tetrahedral resonance with an isotropic shift of 57 ppm represents distorted extraframework aluminum species (Al(IV), EFAl, LAS) [29,30]. There are also two types of octahedral

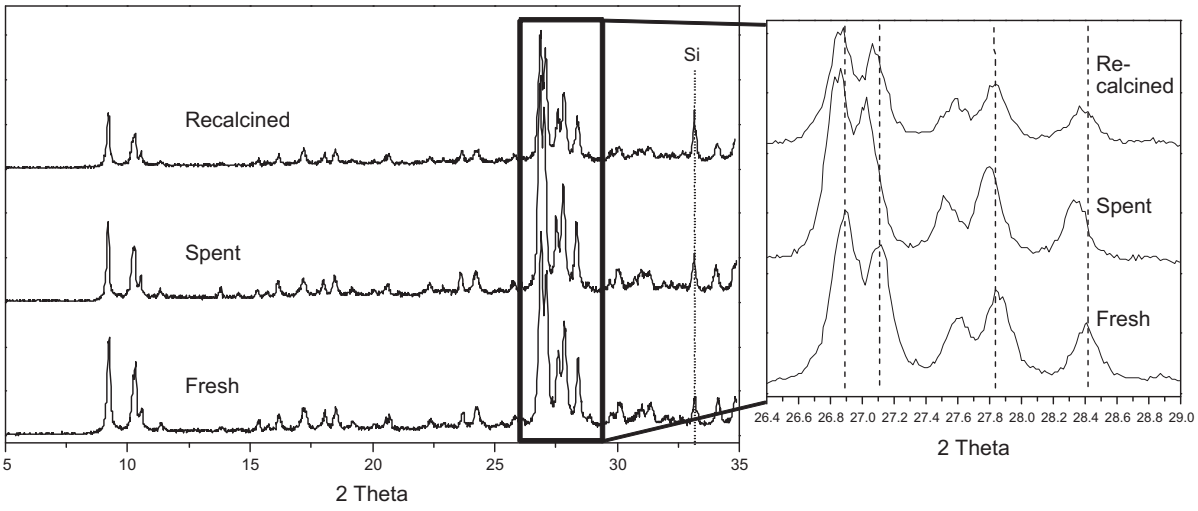

Fig. 6. Top: XRD powder diffraction patterns of a fresh Ru/H-ZSM5 catalyst, after reaction in 2-ethylhexanoic acid (EHA), and after recalcination. Silicon (NBS 640) was used as internal standard by physical mixing.

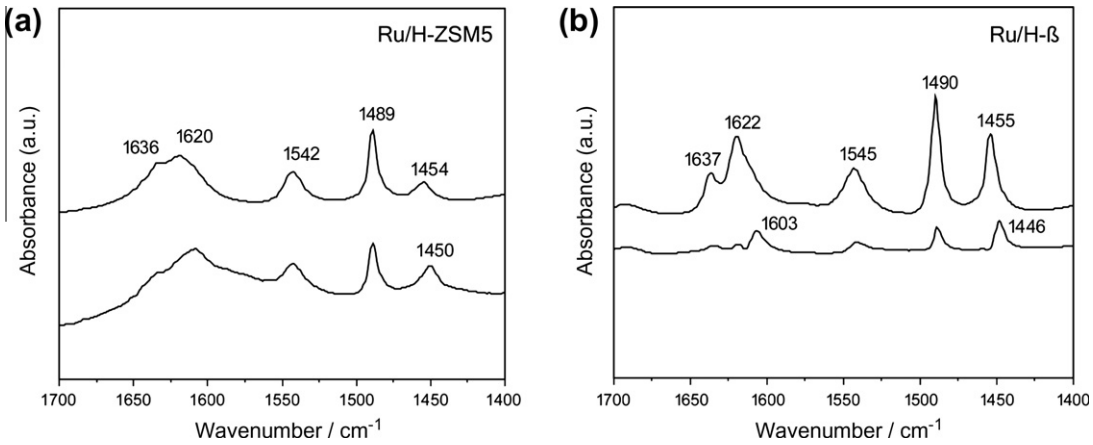

Fig. 7. FT-IR absorbance spectra of adsorbed pyridine of (a) Ru/H-ZSM5 and (b) Ru/H-β (top: fresh catalyst; bottom: spent catalyst after reaction in 2-ethylhexanoic acid).

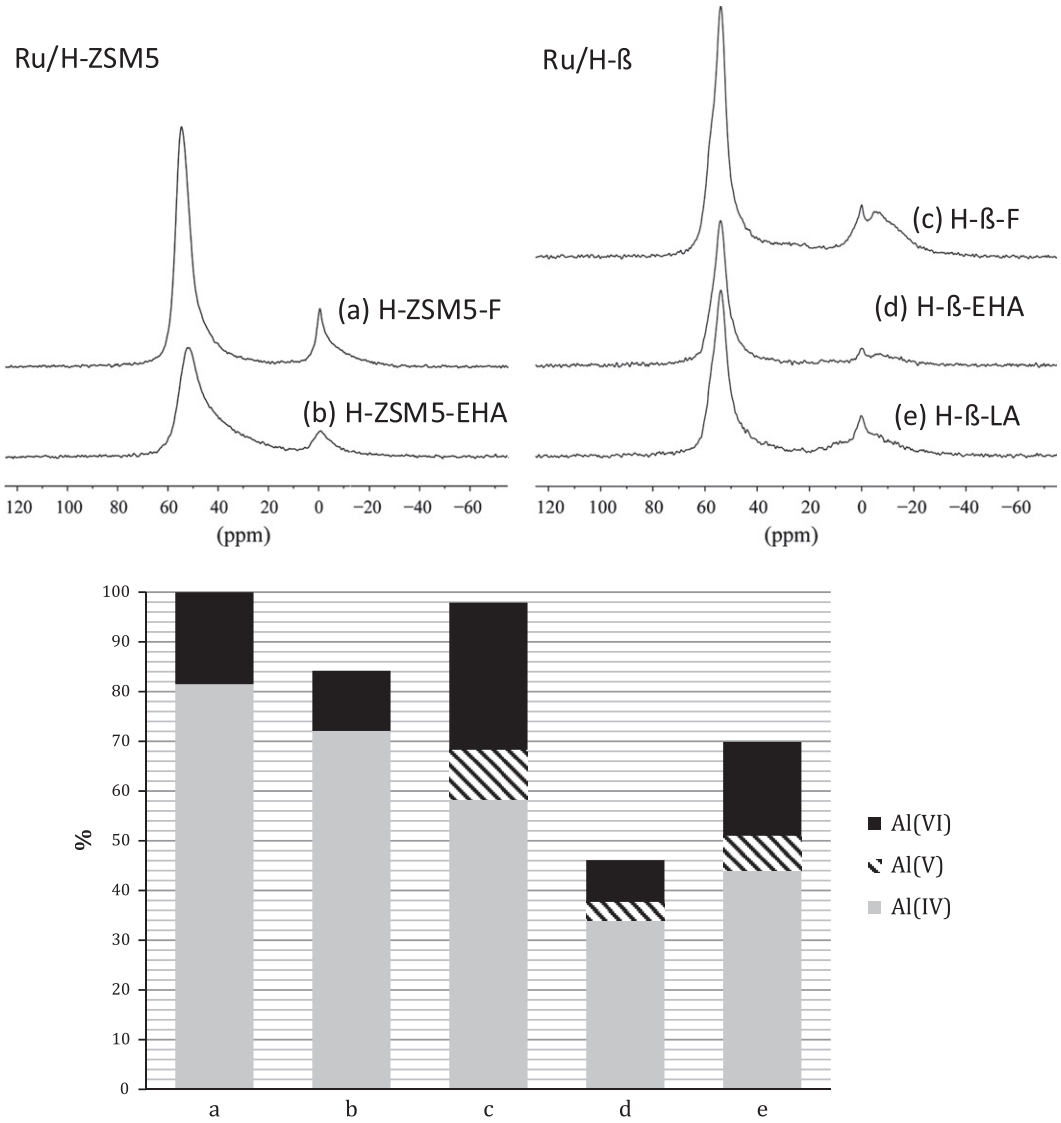

Fig. 8. Top: ^{27}Al MAS NMR spectra of fresh and spent Ru catalysts. (a) Fresh Ru/H-ZSM5; (b) spent Ru/H-ZSM5 (reaction in 2-ethylhexanoic acid for 10 h); (c) fresh Ru/H-β; (d) spent Ru/H-β (reaction in 2-ethylhexanoic acid for 10 h); (e) spent Ru/H-β (reaction in neat levulinic acid for 10 h). Bottom: relative amounts of tetrahedral, penta- and octahedral coordinated aluminum normalized to the aluminum content in the fresh Ru/H-ZSM5 catalyst as determined by ^{27}Al MAS NMR (accuracy ±2%).

aluminum to be seen: a narrow line originating from octahedral aluminum (Al(VI), EFAl, LAS) in a highly symmetric environment, such as for instance $Al(OH)_3{\cdot}3H_2O$ in addition to a broad octahedral resonance also at 0 ppm that has been assigned to extra framework

Table 5
Unit cell lattice parameters of the 1 wt% Ru/H-ZSM5 catalyst before and after reaction and after regeneration.

Ru/H-ZSM5 samples	Lattice constants (Å)		
	a	*b*	*c*
Fresh	20.100	19.909	13.376
Spent	20.100	19.957	13.419
Recalcined	20.101	19.924	13.399

aluminum by some [31], but others have referred to this as framework Al(VI) (Fig. 8a and b) [32,33].

The distorted tetrahedral aluminum is much more prevalent than the tetrahedral framework Al in the spent Ru/H-ZSM5 which shows that conversion of FAl to EFAl sites takes place during the reaction in the hot acid EHA. Not only is tetrahedral FAl converted to EFAL, but there is also an overall decrease in the amount of aluminum as seen by the decrease in intensity of the spectra. The dealumination is more severe for the octahedral species than for the tetrahedral aluminum (Al(IV): 12% decrease, Al(VI): 35% decrease). The loss of acid sites for Ru/H-ZSM5 after reaction is also indicated by the pyridine adsorption data (Fig. 7). Moreover, the reduction in tetrahedral FAL coincides with the reduction in intensity of the 1542 cm^{-1} FTIR line, both pointing toward a reduction in the number of BAS. At the same time, the increase in tetrahedral EFAL together with growth of the band at 1450 cm^{-1} both support an increase in LAS.

The ^{27}Al MAS NMR spectra of the Ru/H-β samples are shown in Fig. 8c–e. In the fresh Ru/H-B sample (Fig. 8c), three tetrahedral species can be discerned in the MQMAS. However, these are severely overlapping in the 1D MAS spectra. The tetrahedral region consists of both FAL and EFAL aluminum. As in ZSM-5, two octahedral species can be detected, both with an isotropic shift around 0 ppm, one type in a highly symmetric environment and one more distorted. Trace amounts of penta-coordinated aluminum species Al(V), with a peak center at 33 ppm, are also detected in the ^{27}Al 3QMAS NMR (Fig. S11) [34,35]. After 10 h of reaction in EHA, dealumination is illustrated by the decrease in intensity of all peaks (Fig. 8d) with a very sharp decrease in six-coordinated suggesting the loss of both FAl and EFAl species (after 10 h reaction in EHA, Al(IV): 41%, Al(V): 64%, Al(VI): 72% decrease. The ^{27}Al NMR spectrum of the reaction of Ru/H-β in neat levulinic acid (NLA, see below) shows that the loss of acid sites in NLA is less severe than in EHA (after 10 h in NLA, Al(IV): 25%, Al(V): 30%, Al(VI): 36% decrease). This can be attributed to the larger total amount of acid used (54 g EHA + 6 g LA vs. 20 g LA in the NLA run) and the fact that in the NLA run, the acid reacts away to form GVL. The ^{27}Al NMR spectra agree with the pyridine data as they both reflect the loss of BAS as well as LAS for Ru/H-β.

H-β is thus more easily dealuminated than H-ZSM5 in the presence of the hot acid EHA. Müller et al. already showed that H-β was more easily dealuminated than H-ZSM5 by a hydrothermal treatment in the presence of oxalic acid [36]. The severe dealumination of H-β corresponds with the lower yield of PA in the EHA runs with Ru/H-β as compared to Ru/H-ZSM5 (Fig. 4). The continuous loss of acid sites of Ru/H-β hampers the GVL to PEA conversion (Scheme 1). Although Ru/H-ZSM5 suffers more from sintering and coke formation (Table 2), less acid sites are lost, resulting in a higher PA yield in EHA.

3.4. Catalytic reactions in neat levulinic acid

3.4.1. Catalyst performance

The acidity of the support was also shown to influence activity and selectivity in the catalytic hydrogenation of neat LA by Ru/TiO_2 or Ru/H-β (Table 6). Indeed, Ru/H-β showed higher activity for the hydrogenation of LA. Reaching full conversion with 0.3 g Ru/H-β in 4 h (TOF > 0.403 s^{-1}) (Table 6, entry 4), compared to 57.8% LA conversion with 0.3 g Ru/TiO_2 (TOF = 0.233 s^{-1}) (Table 6, entry 1). Conversion could be increased to 98.1% after 4 h when 0.5 g Ru/TiO_2 was used (TOF = 0.239 s^{-1}) (Table 6, entry 2). These results are similar to those reported by Manzer for the conversion of neat LA using a 5 wt% Ru/Al_2O_3 catalyst at 473 K and 33.4 bar hydrogen (TOF = 0.405 s^{-1}, only high conversion data available) [37]. Palkovits et al. recently showed that full conversion of neat LA can also be achieved with Ru/C (5 wt%) at very mild conditions (298 K, 12 bar H_2), but at the longer reaction time of 50 h [9]. A comparison of TOF numbers shows that the LA to GVL conversion is accelerated by the acid sites on Ru/H-β; the TOF numbers obtained in neat LA runs are larger than those of the EHA runs (Ru/TiO_2: 0.239 vs. 0.164; Ru/H-β: >0.403 vs. 0.131), illustrating that the substrate LA competes with the solvent EHA for adsorption on the catalyst. Minute amounts of the deeper hydrogenation products PD, PA, and MTHF were observed with Ru/TiO_2 (Table 6, entry 3), while higher but still low yields of PA were achieved with Ru/H-β with the yields increasing with catalyst amount and reaction time. PD was not observed in the runs with Ru/H-β (Table 6, entries 4–6).

3.4.2. Catalyst stability in neat levulinic acid

Interestingly, both very limited sintering (Fig. S5) and limited Ru loss (Table 3) were observed with Ru/TiO_2 in pure LA. Ru/TiO_2 thus showed good stability not only in dioxane, but also under more severe conditions such as in EHA or in neat LA. Some sintering was observed with Ru/H-β as in EHA, but less Al was lost to the liquid phase compared to the EHA runs, which can again be attributed to the disappearance of the acid function upon conversion of LA to GVL. No phase change occurred for both supports (Fig. S8). A very small drop in surface area was found for the titania catalyst, consistent with the limited formation of coke that was observed by TGA. More coke formed on the acidic catalyst, resulting in a larger drop in surface area and pore volume. More coke was deposited on both catalysts in neat LA than in EHA (Ru/H-β: 10.7 vs. 3.4 wt%; Ru/TiO_2: 1.8 vs. 0.8 wt%), illustrating that a LA derivative and not EHA is the precursor for coke formation (Table 2).

4. Conclusions

Our study demonstrates that the catalytic performance of the four supported Ru catalysts for the hydrogenation of levulinic acid (LA) is greatly affected by the nature of the support and the solvent

Table 6
Catalytic performances for the hydrogenation of neat levulinic acid (LA) with GVL, γ-valerolactone; PA, pentanoic acid; MTHF, methyltetrahydrofuran and PD, 1,4-pentanediol.

Entry	Catalyst	Time (h)	Catalyst amount (g)	C-balance	LA conv. (%)	GVL yield (%)	PA yield (%)	MTHF yield (%)	PD yield (%)
1	Ru/TiO_2	4	0.3	100.4	57.8	57.8	0.3	0.1	0.0
2	Ru/TiO_2	4	0.5	99.6	98.8	97.7	0.4	0.2	0.1
3	Ru/TiO_2	10	0.5	98.9	100.0	97.5	0.4	0.4	0.6
4	Ru/H-β	4	0.3	92.8	100.0	91.0	1.7	0.1	0.0
5	Ru/H-β	4	0.5	91.7	100.0	89.2	2.3	0.2	0.0
6	Ru/H-β	10	0.5	91.3	100.0	86.6	4.0	0.7	0.0

Conditions: 473 K, 40 bar, 0.3 g 1 wt% Ru catalyst, stirrer speed of 1600 rpm, 20 g LA.

choice. The non-acidic catalyst materials selectively gave γ-valerolactone (GVL) as the main and final product, while the zeolite-supported acidic catalyst proved capable of the direct conversion of LA to pentanoic acid (PA) under relatively mild conditions in dioxane as solvent. The strongly acidic sites on the support material accelerate the LA to GVL conversion and are essential for the subsequent, most difficult step in the sequence, that is, the ring-opening step in the conversion of GVL to PA. PA can also be obtained under more severe conditions, using 2-ethylhexanoic acid or neat LA as solvent, but yields dropped as a result of gradual deactivation of the zeolite-supported catalysts. Although many factors may influence the deactivation of the catalyst material, pyridine adsorption and solid-state ^{27}Al NMR data clearly show that the deactivation of the catalyst materials can mainly be attributed to loss of acid sites by dealumination. It was found that H-ZSM5 was more resistant to dealumination than H-β. Most coke is formed on the zeolite-supported catalyst materials in neat LA, with XRD indicating preferential coke buildup in the zigzag channels of H-ZSM5. The results also show that angelicalactone (AL) is involved as an intermediate in the hydrogenation reaction and that it is a direct precursor for the coke that is deposited mostly on the acidic catalysts. Ru/TiO_2 proved to be remarkably stable and selective for GVL formation, also in the reactions in neat LA with very limited coke formation, sintering and leaching of ruthenium being observed. Further studies on the stability of the mainly the acid sites in the zeolite-supported catalysts, under the highly polar and corrosive conditions of LA conversion, should improve the performance of these first promising examples for the direct conversion of LA to PA.

Acknowledgments

The authors gratefully thank the Smart Mix Program of the Netherlands Ministry of Economic Affairs and the Netherlands Ministry of Education, Culture and Science within the framework of the CatchBio Program. Cor van de Spek is acknowledged for the TEM measurements. The authors thank the CatchBio User Committee for their valuable suggestions and discussions. Support of NWO for the "Solid-State NMR facility for Advanced Materials Science" is gratefully acknowledged. We would like to thank Hans Janssen, Gerrit Janssen and Jan van Os for technical support.

Appendix A. Supplementary material

Supplementary data associated with this article can be found, in the online version, at http://dx.doi.org/10.1016/j.jcat.2013.02.003.

References

[1] B. Girisuta, L.P.B.M. Janssen, H.J. Heeres, Chem. Eng. Res. Des. 84 (2006) 339–349.
[2] D.W. Rackemann, W.O.S. Doherty, Biofuels, Bioprod. Biorefin. 5 (2011) 198–214.
[3] A. Corma, S. Iborra, A. Velty, Chem. Rev. 107 (2007) 2411–2502.
[4] J.J. Bozell, L. Moens, D.C. Elliott, Y. Wang, G.G. Neuenscwander, S.W. Fitzpatrick, R.J. Bilski, J.L. Jarnefeld, Resour. Conserv. Recyc. 28 (2000) 227–239.
[5] I.T. Horvath, H. Mehdi, V. Fabos, L. Boda, L.T. Mika, Green Chem. 10 (2008) 238–242.
[6] J.-P. Lange, R. Price, P.M. Ayoub, J. Louis, L. Petrus, L. Clarke, H. Gosselink, Angew. Chem. Int. Ed. 49 (2010) 4479–4483.
[7] J.C. Serrano-Ruiz, D. Wang, J.A. Dumesic, Green Chem. 12 (2010) 574–577.
[8] Z.-p. Yan, L. Lin, S. Liu, Energy Fuels 23 (2009) 3853–3858.
[9] M.G. Al-Shaal, W.R.H. Wright, R. Palkovits, Green Chem. 14 (2012) 1260–1263.
[10] L.E. Manzer, Appl. Catal. A: Gen. 272 (2004) 249–256.
[11] R.A. Bourne, J.G. Stevens, J. Ke, M. Poliakoff, Chem. Commun. (2007) 4632–4634.
[12] D.C. Elliott, J.G. Frye, US Patent 5883266, Battelle Memorial Institute, 1999.
[13] J.-P. Lange, US Patent 2011/0112326, Shell International B.V., 2011.
[14] P.J. Van den Brink, K.L. Von Hebel, J.-P. Lange, L. Petrus, WO/2006/[067171], Shell International B.V., 2006.
[15] J.Q. Bond, D.M. Alonso, D. Wang, R.M. West, J.A. Dumesic, Science 327 (2010) 1110–1114.
[16] J.Q. Bond, D.M. Alonso, R.M. West, J.A. Dumesic, Langmuir 26 (2010) 16291–16298.
[17] E. Lippmaa, A. Samoson, M. Magi, J. Am. Chem. Soc. 108 (1986) 1730–1735.
[18] G.L. Woolery, G.H. Kuehl, H.C. Timken, A.W. Chester, J.C. Vartuli, Zeolites 19 (1997) 288–296.
[19] A. Primo, P. Concepcion, A. Corma, Chem. Commun. 47 (2011) 3613–3615.
[20] P.M. Ayoub, J.-P. Lange, WO2008/142127, Shell International B.V., 2008.
[21] D. Di Mondo, D. Ashok, F. Waldie, N. Schrier, M. Morrison, M. Schlaf, ACS Catal. 1 (2011) 355–364.
[22] J. Kornatowski, W.H. Baur, G. Pieper, M. Rozwadowski, W. Schmitz, A. Cichowlas, J. Chem. Soc., Faraday Trans. 88 (1992) 1339–1343.
[23] C.S. Triantafillidis, A.G. Vlessidis, L. Nalbandian, N.P. Evmiridis, Micropor. Mesopor. Mater. 47 (2001) 369–388.
[24] T. Barzetti, E. Selli, D. Moscotti, L. Forni, J. Chem. Soc., Faraday Trans. 92 (1996) 1401–1407.
[25] E.P. Parry, J. Catal. 2 (1963) 371–379.
[26] T. Yashima, N. Hara, J. Catal. 27 (1972) 329–333.
[27] A. Martin, U. Wolf, S. Nowak, B. Lücke, Zeolites 11 (1991) 85–87.
[28] J.P. Marques, I. Gener, P. Ayrault, J.C. Bordado, J.M. Lopes, F. Ramôa Ribeiro, M. Guisnet, Micropor. Mesopor. Mater. 60 (2003) 251–262.
[29] D. Freude, H. Ernst, I. Wolf, Solid State Nucl. Magn. Reson. 3 (1994) 271–286.
[30] E. Brunner, H. Ernst, D. Freude, T. Fröhlich, M. Hunger, H. Pfeifer, J. Catal. 127 (1991) 34–41.
[31] J. Kanellopoulos, A. Unger, W. Schwieger, D. Freude, J. Catal. 237 (2006) 416–425.
[32] Z. Yu, A. Zheng, Q. Wang, L. Chen, J. Xu, J.-P. Amoureux, F. Deng, Angew. Chem. Int. Ed. 49 (2010) 8657–8661.
[33] E.R.H. van Eck, J.A.Z. Pieterse, A.P.M. Kentgens, Solid State Nucl. Magn. Reson. 39 (2011) 99–105.
[34] J.-P. Gilson, G.C. Edwards, A.W. Peters, K. Rajagopalan, R.F. Wormsbecher, T.G. Roberie, M.P. Shatlock, J. Chem. Soc., Chem. Commun. (1987) 91–92.
[35] J. Chen, T. Chen, N. Guan, J. Wang, Catal. Today 93–95 (2004) 627–630.
[36] M. Muller, G. Harvey, R. Prins, Micropor. Mesopor. Mater. 34 (2000) 135–147.
[37] L.E. Manzer, US Patent 2006100449, E. I. Du Pont de Nemours and Company, 2006.